Emergent Materials
https://doi.org/10.1007/s42247-020-00108-y

ORIGINAL ARTICLE

Fabrication of metallic nanonetworks via templated electroless plating as hydrogenation catalyst

Yu-Cheng Chien[1] · Liang-Yu Huang[2] · Kai-Chieh Yang[1] · Mohan Raj Krishnan[1] · Wei-Song Hung[3] · Jing-Cherng Tsai[2] · Rong-Ming Ho[1]

Received: 6 January 2020 / Accepted: 16 May 2020

Abstract

Herein, we aim to suggest a facile method for fabrication of Ni-based nanonetworks via templated electroless plating using mesoporous polymers as templates. With the control of spinodal decomposition for the polymer/crystalline solvent mixture, it is feasible to fabricate mesoporous polystyrene with controlled porosity and pore size as well as its distribution that could serve as a template for templated electroless plating. By taking advantage of the development of reduced Ni from the electroless plating, nanoporous Ni spheres with controlled micrometer-sized particle could be directly acquired, providing the feasibility as heterogeneous catalysts in aimed reactions. With the high specific surface area, the fabricated nanonetwork Ni gave rise to superior performance for catalytic hydrogenation of unsaturated organics and polymers. With the magnetic properties of Ni, catalyst recyclability could be simply achieved by magnetic field. This approach is simple and cost-effective to create nanoporous Ni spheres with high catalytic efficiency and well selectivity for hydrogenation performance.

Keywords Templated electroless plating · Mesoporous polymer · Metallic nanonetwork texture · Hydrogenation catalyst · Polymeric hydrogenation

1 Introduction

In recent decades, metal nanostructures (including noble metal like Au [1, 2], Ag [3–5], Pd [6–12], and Pt [8, 13–18]) have attracted a lot of attention in catalytic applications due to their excellent activity, superior durability, and good recyclability. The performance of heterogeneous metallic catalyst is highly dependent upon the design of nanostructures and morphology [19–21]. Hence, how to synthesize the metal nanocrystals with desirable texture and size has become a principle target of extensive researches on catalytic materials. Recently, various strategies for the fabrication of metallic catalyst with specific morphology, structure, and size have been proposed for providing superior activity [12, 22, 23]. For example, Kiwi-Minsker et al. have successfully controlled the morphologies and sizes of palladium nanocrystals through the change of reaction conditions in the aqueous solution to achieve the selective hydrogenation of 2-methyl-3-butyn-2-ol (MBY) in the reaction [24]. Moreover, Zhang et al. proposed a facile soft chemistry method to fabricate the Ni/CB (carbon black) catalyst by using nickel chloride as the source. That catalyst exhibited high activity for the cost-effective hydrogenation of nitrophenols to aminophenols at 30 °C, and it could be easily separated from the solution after hydrogenation reaction by external magnetic field due to the magnetic property of nickel [25].

It is also very important to determine how to increase both the specific surface area to mass ratio and the amounts of catalytic sites of metallic nanocrystals to enhance the catalytic performance over the hydrogenation reaction. Therefore, the fabrication of three-dimensional (3D) nanoporous materials

Yu-Cheng Chien and Liang-Yu Huang contributed equally to this work.

Electronic supplementary material The online version of this article (https://doi.org/10.1007/s42247-020-00108-y) contains supplementary material, which is available to authorized users.

✉ Rong-Ming Ho
rmho@mx.nthu.edu.tw

[1] Department of Chemical Engineering, National Tsing Hua University, Hsinchu 30013, Taiwan, Republic of China

[2] Department of Chemical Engineering, National Chung Cheng University, Chiayi 62102, Taiwan, Republic of China

[3] Department of Chemical Engineering and R&D Center for Membrane Technology, Chung Yuan Christian University, Taoyuan, Taiwan, Republic of China

Published online: 03 June 2020

with interconnected network structure is in strong demand due to their high specific surface areas and porosity from the nanonetwork texture with nano-pores. With highly porous nanostructures, the catalytic performance and selectivity of metallic nanocrystals would be enhanced, and it also can reduce the consumption of noble metals to achieve the goal of cost-effectiveness. Lately, Huang et al. fabricated uniform porous palladium nanostructures (pPdNs) with perpendicular pore channels by using a convenient wet-chemical strategy. That catalyst exhibited superior efficiency for the hydrogenation of nitrobenzene, styrene, and also a Suzuki coupling reaction because of its uniformly dendritic nanostructures, ultrathin branches, and the high percentage of surface atoms [6]. Moreover, as previously reported by our laboratory, nanonetwork-structured polystyrene (PS) template could be fabricated from either hydrolyzing self-assembled PS-PLLA [26, 27] or HF etching of PS-PDMS [28], which could be used for the fabrication of double gyroid (DG)-structured [29] and single gyroid (SG)-structured [30] Ni through templated electroless plating. With a well-ordered nanonetwork texture, continuous nanochannels, high specific surface area, and a narrow pore size distribution, the SG-structured Ni sphere fabricated from the templated electroless plating exhibits excellent efficiencies to mediate hydrogenation of organic compounds. Note that a well catalyst also should be recovered easily after catalytic reactions. The SG-structured Ni could be separated from the solution after hydrogenation reactions by the external magnetic field due to its magnetic property and micrometer size.

Herein, we aim to fabricate the metallic (i.e., Ni) catalyst with nanonetworked structure and controlled pore size by a facile and cost-effective method. By taking advantage of spinodal decomposition for a mixture of PS and dimethylformamide (DMF) [31], it is possible to fabricate mesoporous PS with a variety of pore sizes by changing the concentration and molecular weight of the PS in the solution mixture. Subsequently, the mesoporous PS will be used as a template for the fabrication of nanonetwork-structured Ni sphere with thru-pore texture and uniform pore size. By taking advantage of the nucleation and growth mechanism for the reduction of Ni ions, nanoporous Ni spheres with different spherical particle sizes can be successfully fabricated for use as metallic nanoporous hydrogenation catalyst. Also, the micrometer-scale size of the nanoporous Ni sphere is critical to provide the excellent recyclability from the reaction solution by simply using an external magnetic field [32, 33]. Hydrogenation catalysts have found important applications in food chemistry, petrochemistry, and pharmaceutical industries. To probe the catalytic behaviors of the novel nanoporous catalyst, hydrogenation of aliphatic (e.g., cyclohexene) and aromatic (e.g., toluene) double bonds was examined, respectively, so that the hydrogenation selectivity of the catalyst can be revealed. In addition, we also studied the hydrogenation of polymeric materials, a commercial thermoplastic elastomer, polystyrene-*b*-polybutadiene-*b*-polystyrene (SBS), using the novel catalyst system for demonstration of its applications on polymers; note that the SBS contains both aliphatic and aromatic double bonds and it is promising for practical applications as the hydrogenated rubber offers elevated physical properties and applications.

2 Experimental section

2.1 Materials

Cyclohexene (≥ 99%) and polystyrene (PS) with three different molecular weights of 190,000, 280,000, and 350,000 were purchased from Sigma-Aldrich®. Dimethylformamide (DMF) was purchased from J.T. Baker®. Methanol and dichloromethane (DCM) were purchased from Macron Fine Chemicals™. Nickel chloride ($NiCl_2{\cdot}6H_2O$) and hydrazine monohydrate (98+%) were purchased from Alfa Aesar. Ammonia, toluene, and hydrofluoric acid (≥ 37%) were purchased from Honeywell. Palladium (II) chloride ($PdCl_2$) was purchased from Uni Region Bio-Tech. The SBS materials in this study were provided by LCY Chemical Corp., Taiwan, and have molecular weights of about 69,000.

2.2 Fabrication of nanoporous Ni spheres via electroless plating

To fabricate the nanoporous Ni spheres, electroless plating was conducted through nucleation and growth. For nucleation process, the mesoporous PS templates were soaked into an activating solution consisting of PdCl2 (0.03 g), methanol (18 mL), and HCl (1 N, 2 mL) at ambient temperature for 24 h followed by immersion in a reduction solution of methanol (15 mL) and hydrazine monohydrate (98+%, 10 mL). After that, the templates with the Pd nucleus were soaked into a Ni bath (0.4 g of nickel chloride (NiCl2·6H2O) dissolved in a solution mixed with distilled water (40 mL), methanol (40 mL), hydrazine monohydrate (98+%, 4 mL), and ammonia (6.4 mL) to grow the Ni. To acquire the free-standing nanoporous Ni spheres, the PS/Ni networked nanohybrids were washed with dichloromethane to remove the mesoporous PS templates.

2.3 Field emission scanning electron microscopy

To acquire field emission scanning electron microscopy (FESEM) images, energy-dispersive X-ray spectroscopy (EDX), and element mapping, the nanoporous Ni sphere powder was prepared after the mesoporous PS template was removed. A HITACHI SU-8010 field emission scanning

electron microscope was used for FESEM imaging at accelerating voltages of 10 keV.

2.4 Transmission electron microscopy

To obtain transmission electron microscopy (TEM) images, the nanoporous Ni spheres in the PS templates were prepared by microtomy, and the nanoporous Ni spheres were dispersed in the methanol followed by dropping on the copper grid. A JEOL JEM-2100 LaB6 transmission electron microscope was used for TEM imaging at an accelerating voltage of 200 kV.

2.5 Pore size and isotherm measurements

The pore size, porosity, and isotherms of the fabricated mesoporous PS bulk were investigated using a volumetric gas adsorption apparatus (BET Sorptometer, CBET-201A, PMI, USA). Fill pieces of dried sample into a glass sample tube and thoroughly dried under vacuum at 50 °C overnight. The specific surface area of the PS bulks was analyzed from the Brunauer-Emmett-Teller (BET) method, and the pore size distribution was acquired from Barrett-Joyner-Halenda (BJH) analysis. The hysteresis was obtained between adsorption and desorption processes, which is often the phenomenon for the mesoporous materials with capillary condensation.

2.6 Hydrogenation reactions

Hydrogenation of cyclohexene and toluene was conducted in a 100-mL Parr reactor using decalin as the diluent. The hydrogenation reactions were conducted at 80 or 200 °C under 50 atm of hydrogen for 4 h. The ratio of hydrogenation conversion was determined by ^{1}H NMR analyses. The hydrogenation of SBS rubber (M_n = 69,000 g/mol with 5 wt% in cyclohexane) were conducted in a 1000-mL Parr reactor under 50 bar of hydrogen at 200 °C for 4 h. The ratio of hydrogenation conversion was also determined by ^{1}H NMR analyses.

2.7 Demonstration of the recyclability of nanoporous Ni spheres

As demonstrated in Video S1, 200 mg of nanoporous Ni spheres in powder form used in the catalytic hydrogenation reactions was dispersed in 200 mL of SBS solution (5 wt% in cyclohexane). The nanoporous Ni catalyst powders can be easily collected by an external magnetic field, and then, the re-dispersion of the collected Ni catalyst powders can be achieved by the shearing force. The dispersion and collection of the nanoporous Ni sphere powders can be easily repeated without any limitation.

3 Results and discussion

3.1 Fabrication and identification of mesoporous PS templates

As shown in Fig. 1, the schematics illustrate the experimental procedures for the fabrication of the nanoporous Ni spheres in this study. Following the successful approach developed by Ichinose's group [31], nanonetwork-structured PS template with mesopores (Fig. 1(a)) could be successfully fabricated through spinodal decomposition. To acquire the fabrication method of the mesoporous PS with controlled pore size, porosity, and framework size, PS samples with different molecular weights were used to dissolve in DMF at various concentrations for phase separation through specific cooling and heating processes. With the morphological evolution from spinodal decomposition, co-continuous network texture for PS and crystalline DMF could be obtained in mass production. After extraction of the crystalline DMF, mesoporous PS was thus fabricated. As shown in Figs. S1-S3, the FESEM micrographs show the mesoporous PS with nanonetwork-structured texture at which the forming nanochannels could provide excellent mass transport for the pore-filling of Pd ion solution; after reduction, homogeneously distributed Pd nanoparticles (Fig. 1(b)) could be fabricated. The PS templates with mesopores were well characterized by the nitrogen sorption isotherms (type IV) of BET measurements (Fig. S4 and Table S1). Following the platform technology for templated electroless plating we developed, reduction of Ni could be carried out through the growth of reduced Ni from the Pd nanoparticles as nuclei (Fig. 1(c)). After removal of the PS template, nanonetwork-structured Ni could be obtained (Fig. 1(d)) at which the forming size as sphere can be well controlled by the growth time for the reduction of Ni ions. Figure 2 shows the plot of the framework size of the mesoporous PS fabricated versus the concentration of PS with different molecular weights in the DMF solution. Note that the framework sizes of the mesoporous PS were measured by examination of the FESEM micrographs using the ImageJ software (see SI for details). As shown, the framework size increases approximately linearly with the concentration of the DMF solution. We speculate that the enlargement of the framework size is attributed to the reduction in the amount of the DMF (i.e., the porosity), giving rise to the decrease on the pore size of the mesoporous PS at the same degree of spinodal decomposition. Note that the framework of aimed nanonetwork-structured Ni will be dependent upon the pore size of the mesoporous PS; namely, the pore size of the nanoporous Ni should be the framework size of the mesoporous PS. Surprisingly, with the discrepancy on the concentration for only 10%, the framework size could be changed to two times of the original size, giving the effective way for the control of the pore size of the nanoporous Ni. In addition to the

control of concentration, it is also possible to achieve the transformation of framework size (i.e., the pore size of fabricated nanoporous Ni) by varying the molecular weight of the PS; as shown in Fig. 2, the framework size will increase with the increase of molecular weight. We speculate that, with the increase of PS molecular weight, the large PS molecular weight might lower the mobility of the DMF in the PS and also reduce the miscibility of PS in the DMF. Owing to the reduced mobility during the temperature increasing procedure from the temperature of liquid nitrogen, less amounts of DMF in the mixture for spinodal decomposition (that is, the lower porosity for the fabricated mesoporous PS); on the other hand, the lower miscibility might give rise to the formation of larger PS framework so as to enlarge the pore size for the fabricated mesoporous PS. Because of the bigger pore size and the reduction on porosity (i.e., the amount of the DMF), the specific surface area should be smaller at equivalent degree of spinodal decomposition. Note that it is possible to increase the framework size up to 30 nm by changing the molecular weight from 280,000 to 350,000 g/mol at equivalent concentration (Figs. S2e and S3e). Nevertheless, the nanonetwork structures might not be able to form once the amount of DMF decreases to 60% due to its limited amount of the pore for the formation of the nanonetwork structure.

We speculate that the changes on the interdomain spacing of fabricated mesoporous PS are attributed to the less amounts of DMF solution that will give the small pores at high PS concentration, in line with the imaging results above. During rapid cooling process using liquid nitrogen for quenching followed by the heating process, DMF nanocrystalline could be formed in the PS with the equivalent size first, and then, the growth of the crystalline

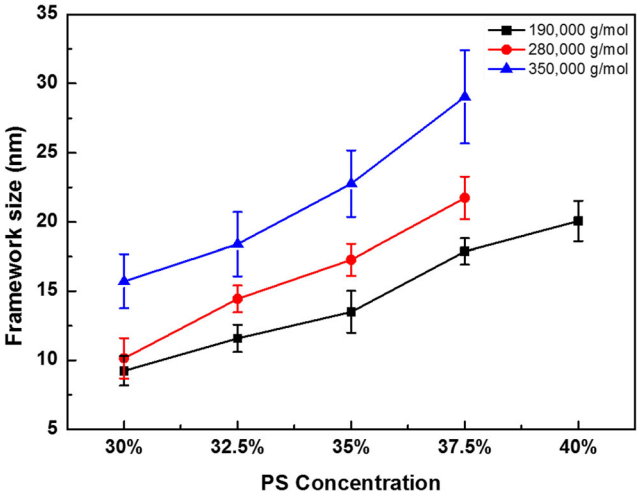

Fig. 2 Plots of the framework size of the mesoporous PS bulk fabricated from spinodal decomposition versus the concentration of PS in the mixture with the molecular weight of PS: 190,000; 280,000; 350,000 g/mol. The framework sizes of PS were measured by examination of SEM images

DMF will define the final morphology to give the pore size of fabricated mesoporous PS. Moreover, the decrease on the mobility and the miscibility of the PS in DMF solution with the increase of the molecular weight might result in the less degree of phase separation that will enlarge the framework sizes of the fabricated mesoporous PS and also the DMF domain size (namely the pore size of the PS). Consequently, the q value of the reflection in the SAXS result of the mesoporous PS becomes smaller, reflecting the increase of the interdomain distance, in line with the imaging results from FESEM observation and the pore size analysis from BET measurements.

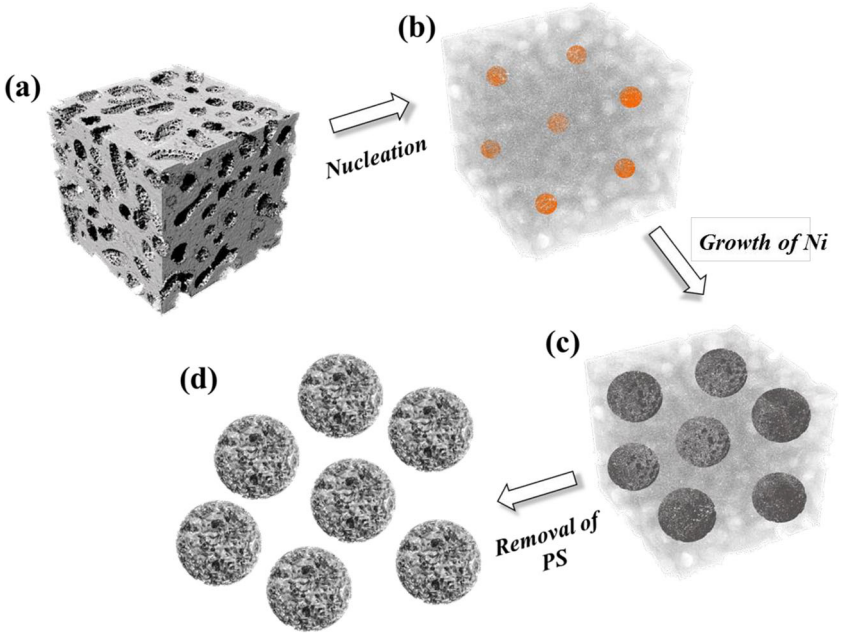

Fig. 1 Schematic illustration for the fabrication of nanoporous Ni spheres from mesoporous PS through templated electroless plating. (a) Mesoporous PS template possessing the interconnect-nanonetworked structure with high specific inner surface area. (b) Pd nanoparticles distributed in the template serving as nuclei for the reduction of Ni ions. (c) PS/Ni nanohybrids with nanonetwork texture via templated electroless plating. (d) Nanonetwork-structured Ni porous spheres fabricated after removal of the PS template

3.2 Synthesis and characterization of nanoporous Ni spheres

As demonstrated by our previous works, nanoporous Ni sphere could be fabricated by templated electroless plating through nucleation and growth processes. By pore-filling Pd^{2+} solution into the nanochannels of mesoporous PS template, homogeneously dispersed Pd nuclei could be formed by using monohydrate hydrazine as a reducing agent. As shown in Fig. S7a, Pd nanoparticles from the reduction of Pd ions could be identified followed by the reduction of Ni ions from the Pd nuclei. With the growth of Ni, micrometer-scale Ni sphere could be clearly observed after removal of the PS template (Fig. 3(a)). Moreover, abundant amounts of micrometer-sized nanoporous Ni spheres could be successfully fabricated, providing the potential for various applications. The inset of Fig. 3(a) shows a photograph of the nanoporous Ni spheres in a black powder form, demonstrating the feasibility for fabrication of a large amount of nanoporous Ni spheres. A high-magnification micrograph of the Ni sphere shows the coral-shaped outer surface, suggesting that reduced Ni becomes the inverse phase of PS template so as to create the outer surface of nanonetwork texture after removal of the PS template (Fig. 3(b)). To further examine the suggested nanonetwork texture, TEM imaging was acquired; as shown in Fig. S7b, the projection of the nanoporous Ni sphere is in line with the SEM results at which the formed Ni appears as dark microdomain with bright projection of the pores. Figure S7c shows the nanonetwork structure inside the nanoporous Ni sphere at high magnification, giving the potential for the hydrogenation of organics and polymers due to its high specific surface area. The crystalline structures of the nanoporous Ni spheres were characterized by a wide angle X-ray diffraction (WAXD) experiment (Fig. S7d); the pattern shows several intense diffraction peaks located at 44.9°, 52.3°, and 76.8°, corresponding to the (111), (200), and (220) reflection planes of a face-centered cubic (fcc) Ni phase.

3.3 Controlled growth of spherical particle size and tunable pore size formation

As shown in Fig. 4(a)–(f), the particle size of the Ni sphere will be dependent upon the reduction time. Note that under specific nucleus density estimated using formula in Section 2.1, there is no significant color change in the first 2 h; based on the TEM observation, the particle size of Ni sphere would be smaller than 100 nm. The particle size of the Ni sphere is approximately 120 nm after 3 h and gradually increases to approximately 1200 nm after 120 h. As shown in Fig. 4(g), a plot shows the relationship between the Ni sphere size, based on the statistical calculation for the average particle size from the FESEM micrographs, and the reaction time; a typical growth pattern for templated electroless plating from the heterogeneous Pd nucleus shows that the growth rate gradually reduces with the increase of the reaction time. Also, the growth rate of nanonetwork-structured nanoporous Ni sphere experiences a reduction on the growth rate after 96 h at which the particle size will reach a maximum plateau even after refreshing the reduction agent and/or introducing new batch Ni ion solution; therefore, the reduction on the growth of Ni spheres might be attributed to the reduction on the mass transport of Ni ions into the mesoporous template.

Positron annihilation spectroscopy (PAS) was conducted to determine the pore size distribution of the nanoporous Ni spheres. A total of 50 mCi of 22Na was served as positron source for the analysis. After implantation of the positron into the nanoporous Ni spheres in powder under ambient conditions, the lifetime of positron was detected (Fig. 5(a)). Within the lifetime being detected, it is possible to acquire the pick-off annihilation rate of o-Ps (ns-1) (λ^R) based on age-momentum correlation (AMOC) technique combining with the selection of the 3γ annihilation located in the range of 340–490 keV analyzed by PATFIT program, giving the fitting of the distribution of the longest o-Ps lifetime (Fig. 5(a)). Consequently, the pore size of the nanoporous Ni spheres was calculated based on the relationship between λ^R and volume radius (R) derived by Tao and co-workers, and further modified

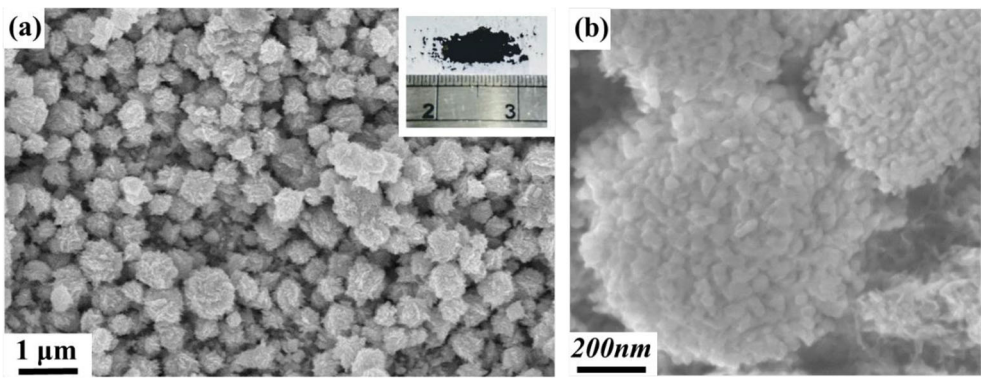

Fig. 3 (a) Low-magnification and (b) high-magnification SEM micrographs of nanonetwork-structured nanoporous Ni spheres from templated electroless plating using mesoporous PS as a template. The inset image shows a photograph of the nanonetwork-structured nanoporous Ni spheres in a powder form

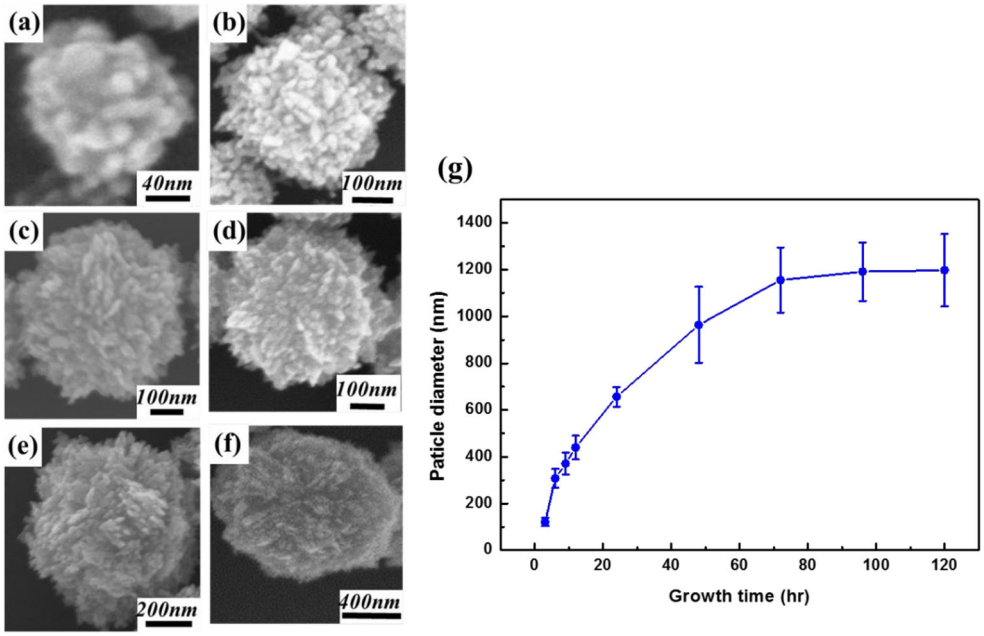

Fig. 4 SEM micrographs of the nanonetwork-structured nanoporous Ni spheres at different growth times for Ni reduction: (a) 3 h; (b) 6 h; (c) 9 h; (d) 12 h; (e) 24 h; (f) 48 h. (g) Plot of the particle radii of the nanonetwork-structured nanoporous Ni spheres versus reduction time for Ni deposition

to Eq. (1) to include 3γ from o-Ps annihilation for the calculation of pore size larger than 1 nm with $\Delta R = 0.166$ nm, Ra = 0.8 nm, and $b = 0.55$ [34, 35]. As shown in Fig. 5(b), based on the calculated pore size distribution, the full width at half of maximum (Dfwhm) could be as low as 3.7 ns, indicating that the nanoporous Ni sphere possesses the pore size of approximately 10.8 nm and 16.8 nm for using the templates with molecular weight of 280,000 g/mol at the concentration of 30% and 35%. These results are in line with the measurements of the framework size (Fig. 2) from FESEM images. Therefore, we could obtain the pore size of the nanoporous Ni sphere through estimating the framework size of the mesoporous PS based on the above experimental results.

$$\lambda^{R} = \begin{Bmatrix} \lambda_{2\gamma}^{R_a}\left[1-\left(\frac{R-R_a}{R+\Delta R}\right)^{b}\right] + \lambda_{3\gamma} \ldots (R \geq R_a) \\ \lambda_{2\gamma}^{R_a} + \lambda_{3\gamma} \ldots\ldots\ldots\ldots\ldots\ldots (R < R_a) \end{Bmatrix} \quad (1)$$

3.4 Exploiting nanoporous Ni spheres for hydrogenation reaction

Owing to its nanoscale pore size, network texture, and controllable micrometer-sized sphere, it is appealing to use the fabricated nanoporous Ni sphere for an extensive variety of applications. Herein, we intend to exploit it as a hydrogenation catalyst for the demonstration of practical application. Ni metal is a commonly used heterogeneous catalyst in hydrogenation reaction. In the heterogeneous catalytic hydrogenation procedures, effective catalysts need to possess not only high catalytic activity but also excellent durability and recyclability. In general, catalytic activity typically depends mainly on the specific surface area and the mass transport procedure. The nanoporous Ni sphere fabricated by electroless plating has been proved to have the fcc crystalline phase; as a result, the packing of atoms in the fcc lattice structure gives the easy absorption of hydrogen, resulting in high activity for organics or polymer hydrogenation on the catalyst surface [36–38].

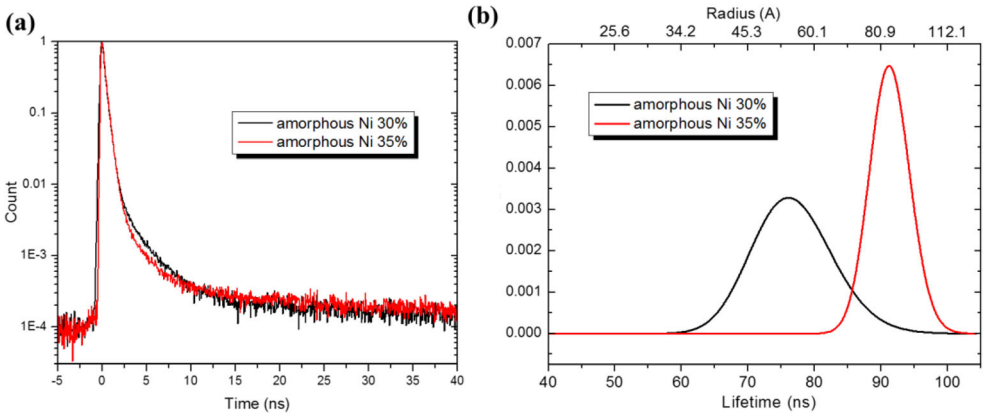

Fig. 5 (a) Age-momentum correlation spectrum (3γ annihilation in the range of 340–490 keV) for the nanonetwork-structured nanoporous Ni sphere powder by using PS with molecular weight of 280,000 g/mol at the concentration of 30% (black line) and 35% (red line). (b) Pore size distribution calculation by positron annihilation spectroscopy using the longest o-Ps lifetime obtained from AMOC

Moreover, with the interconnect-nanonetworked structure having high inner specific surface area, it is reasonable to suppose the high catalytic efficient for hydrogenation reaction. Moreover, the continuous network texture of the nanoporous Ni sphere with mesoscale pore size could enhance the ability for mass transport of the reactants within the nanochannels, which would supply the abundant reaction sides inside the Ni sphere and prevent the unnecessary blocking from the districts with smaller pore size. The catalytic activity of the nanoporous Ni sphere was demonstrated by the hydrogenation of aromatic (i.e., toluene) and aliphatic double bond (i.e., cyclohexene) under different reaction conditions (see Table 1 for details). For the hydrogenation of aromatic double bonds, 95% conversions can be accomplished. This hydrogenation activity is comparable with the hydrogenation results using single gyroid-structured Ni sphere catalyst synthesized as previously reported by our laboratory. Note that the method for the fabrication of such disordered nanonetwork Ni spheres is much more appealing in the practical applications due to its facile and cost-effective approach for the preparation of PS templates, which is indeed much easier than the one generated from gyroid-structured template. The fabrication process (including the preparation of templates and the complexity of templated electroless plating) for the aimed gyroid-structured Ni sphere is much more challenging. Accordingly, the reaction for the hydrogenation of unsaturated double bond was conducted under the condition of 50 bar and 80 °C with the use of 3 mL cyclohexene as reactant by introducing 40 mg catalyst into the reactor.

With the similar reaction condition, in contrast to the commercial Raney® nickel (with a nickel composition of 61%) with only 36% conversion, the conversion for the fabricated nanoporous Ni spheres could reach up to 98%. We speculate that this significant improvement is attributed to the high specific surface area of the nanoporous Ni sphere from the free-standing nanonetwork with the through-pore character that is intrinsically different from the commercial Raney® nickel catalyst, which situated the reactive sites only at the outer surface of the catalyst. Moreover, the nanoporous Ni sphere with high efficiency possesses high selectivity for the hydrogenation between toluene and cyclohexene. Platinum and palladium are well-known excellent catalysts but the hydrogenation of aromatic and aliphatic double bonds might happen simultaneously under the mild reaction conditions [39, 40]. Compared with the noble metal catalysts, such as platinum and palladium, under the mild reaction conditions (i.e., 50 bar and 80 °C), the nanoporous Ni sphere shows the selective hydrogenation of aliphatic double bonds (cyclohexene) with unsaturated double bond but displays no hydrogenation activity toward the aromatic double bonds (toluene). As summarized in Table 1, the nanoporous Ni sphere catalyst displays outstanding hydrogenation activity and selectivity that offers potential industrial applications. We have to point out that, for the use in various industrial processes, the nanoporous Ni sphere catalysts need to maintain its hydrogenation activity after several cycles of catalyst collection and hydrogenation. As shown in Table S2, the hydrogenation of unsaturated double bond was conducted under 50 bar of hydrogen and at 80 °C in the presence of 3 mL cyclohexene as reactant using 40 mg of catalyst. The conversion for the aliphatic double bonds (cyclohexene) is up to 97% in the first reaction cycle, and after several reaction/collection cycles, the hydrogenation ratio can be maintained at 95%. We speculate that the purged hydrogen from previous cycles could be retained in the mesopores of Ni spheres that prevents the oxidation of the Ni catalyst by exposing into the oxygen in the air. Based on the results of catalyst recyclability experiments, the nanoporous Ni spheres is obviously able to maintain high hydrogenation activity after several reaction cycles.

In order to examine the effect of pore size, the nanoporous Ni sphere was used as the catalyst in the hydrogenation of the SBS triblock copolymer. Note that the SBS has a much higher molecular weight as compared with the small organic compound of cyclohexene and toluene; as a result, for effective hydrogenation of SBS, an increase in the pore size of the nanoporous Ni sphere should be critical to give the feasibility to pore fill the polymers into the channels for catalytic reactions as expected. To provide a systematical investigation on the pore size effect, the nanoporous Ni spheres fabricated from the mesoporous PS templates with PS molecular weight of

Table 1 The hydrogenation of aliphatic and aromatic double bonds using nanonetwork-structured nanoporous Ni spheres as catalyst

Entries	Toluene/cyclohexene (mL)	P (bar)	Temp. (°C)	Time (h)	Cat. weight (mg)	Conversion for toluene/cyclohexene
SG-structured Ni spheres	3/0	50	200	4	17	97%/-
Nanoporous Ni spheres	3/0	50	200	4	17	95%/-
Raney® Ni	3/0	50	200	4	17	70%/-
Nanoporous Ni spheres	0/3	50	80	4	40	-/98%
Raney® Ni	0/3	50	80	4	40	-/36%
Nanoporous Ni spheres	1.5/1.5	50	80	4	17	1%/97%
Raney® Ni	1.5/1.5	50	80	4	17	1%/45%

190,000, 280,000, and 350,000 g/mol at 37.5% in the DMF solution were used for the templated electroless plating. The nanoporous Ni spheres were used as catalyst for hydrogenation of 5 wt% SBS in the 200 mL cyclohexane solution under the condition of 50 bar and 200 °C by introducing 200 mg catalyst into the reactor. As shown in Table 2, in contrast to Entry 1, it could be found that the conversions for unsaturated double bond would increase approximately 50% when the pore size is enlarged by using the template from the PS with the M_w of 190,000 g/mol. Moreover, when the nanoporous Ni spheres possess much larger pore size comparing with nanoporous Ni spheres fabricated by the templates from the higher PS molecular weight such as 280,000 and 350,000 g/mol, the conversion of hydrogenation of aromatic double bonds could be also increased. Obviously, the pore size of nanoporous Ni sphere plays an important role in the SBS hydrogenation reaction. The fact that nanoporous Ni sphere catalyst fabricated from higher molecular weight PS shows higher catalytic activity for SBS hydrogenation can be rationalized by higher molecular weight PS template providing larger pore size in the resultant nanoporous Ni sphere catalyst so that offering higher tendency for the high molecular weight SBS polymer to enter into the reactive site containing pore to initiate the hydrogenation reaction. As a result, the conversions for the 1,2 addition butadiene and 1,4 addition butadiene of SBS could reach up to over 90% with the loading amounts of nanoporous Ni sphere from 200 to 350 mg, reflecting that the nanoporous Ni sphere could offer almost complete hydrogenation of aliphatic double bonds. These SBS hydrogenation results indicate that such a heterogeneous catalyst could provide excellent performance on hydrogenation of polymeric materials similar to the type of homogeneous catalysts. Note that one critical advantage for the heterogeneous catalyst is its recyclability; it is essential for a cost-effective process. Owing to the robust structure of the continuous nanonetwork, the texture would be maintained after the hydrogenation reaction, which could be reused after many cycles without significant decay on hydrogenation efficiency. Moreover, based on the micrometer-scale dimension, the nanoporous Ni spheres could be easily suspended in the reactant solution for hydrogenation reaction and then simply recycled by using a magnet to collect the Ni catalyst. After collecting the spheres by applying an external magnetic field, the catalyst could be simply re-dispersed in the suspension by the shearing (see Video S1 for demonstration).

Table 2 The nanonetwork-structured nanoporous Ni spheres for the demonstration of polymeric catalysis performance with different loading amounts

Entries	5 wt% SBS in cyclohexane (mL)	P (bar)	Temp. (°C)	Time (h)	Cat. weight (mg)	Conversion for 1,2 addition butadiene/1,4 addition butadiene/ aromatic ring
1[a]	200	50	200	4	200	28%/28%/21%
2[b]	200	50	200	4	200	42%/41%/25%
3[c]	200	50	200	4	200	42%/41%/31%
4[d]	200	50	200	4	250	59%/49%/49%
5[e]	200	50	200	4	350	93%/91%/59%

[a] 190,000, [b] 280,000, and [c–e] 350,000 (g/mol) of PS at 37.5% in the mixture of PS/DMF used as template for the fabrication of nanoporous Ni sphere which was applied in the polymeric hydrogenation reaction for SBS

4 Conclusions

In summary, the nanoporous Ni sphere with nanonetwork texture can be successfully fabricated by a facile and cost-effective procedure for the templated electroless plating method with mass production. Through controlling the concentrations of PS with different molecular weights in DMF solution, the pore sizes for the templates and thus the nanoporous Ni spheres fabricated from the templated synthesis can be well tuned in the mesoporous region. Moreover, the nanonetwork structure with thru-pore character could be fabricated without additional efforts like templated electroless plating from self-assembled block copolymers with gyroid texture such as the requirement for precise control for Pd concentration to narrow down the pore size distribution. Consequently, the nanoporous Ni spheres with uniform pore sizes, high specific surface areas, and micrometer-scale particle size can be obtained. As demonstrated in this study, the nanoporous Ni sphere displays an excellently catalytic efficiency for organics and polymers for hydrogenation reaction; it also possesses perfect recyclability due to its micrometer-sized particle. As a result, the fabricated nanoporous Ni spheres have high appealing potential for practical applications in the industries because of their nanonetwork texture for pore-filling of reactants, uniform nanoscale-sized pore for high catalytic efficiency, micrometer-sized particle for recyclability, and, most importantly, cost-effective fabrication process for mass production.

Funding information The authors thank the Ministry of Science and Technology, Taiwan, for financially supporting this research under Contract No. MOST 107-2923-M-007-003-MY3, and National Synchrotron Radiation Research Center (NSRRC) for its assistance in the synchrotron SAXS experiments.

Compliance with ethical standards

Conflict of interest The authors declare that they have no conflict of interest.

References

1. T. Hayashi, K. Tanaka, M. Haruta, J. Catal. **178**, 566–575 (1998)
2. C.-H. Hao, X.-N. Guo, M. Sankar, H. Yang, B. Ma, Y.-F. Zhang, X.-L. Tong, G.-Q. Jin, X.-Y. Guo, ACS Appl. Mater. Interfaces **10**, 23029–23036 (2018)
3. C. Kim, Y. Kwon, H. Lee, Chem. Commun. **51**, 12316–12319 (2015)
4. B. Wiley, Y. Sun, Y. Xia, Acc. Chem. Res. **40**, 1067–1076 (2007)
5. V.K. Das, S. Mazhar, L. Gregor, B.D. Stein, D.G. Morgan, N.A. Maciulis, M. Pink, Y. Losovyj, L.M. Bronstein, ACS Appl. Mater. Interfaces **10**, 21356–21364 (2018)
6. X. Huang, Y. Li, Y. Chen, E. Zhou, Y. Xu, H. Zhou, X. Duan, Y. Huang, Angew. Chem. Int. Ed. **52**, 2520–2524 (2013)
7. B. Lim, M. Jiang, P.H.C. Camargo, E.C. Cho, J. Tao, X. Lu, Y. Zhu, Y. Xia, Science **324**, 1302–1305 (2009)
8. V.R. Stamenkovic, B. Fowler, B.S. Mun, G. Wang, P.N. Ross, C.A. Lucas, N.M. Marković, Science **315**, 493–497 (2007)
9. S.-W. Kim, M. Kim, W.Y. Lee, T. Hyeon, J. Am. Chem. Soc. **124**, 7642–7643 (2002)
10. J.P. Wolfe, R.A. Singer, B.H. Yang, S.L. Buchwald, J. Am. Chem. Soc. **121**, 9550–9561 (1999)
11. A. Balouch, A. Ali Umar, A.A. Shah, M. Mat Salleh, M. Oyama, ACS Appl. Mater. Interfaces **5**, 9843–9849 (2013)
12. C. Li, M. Iqbal, B. Jiang, Z. Wang, J. Kim, A.K. Nanjundan, A.E. Whitten, K. Wood, Y. Yamauchi, Chem. Sci. **10**, 4054–4061 (2019)
13. C. Wang, H. Daimon, T. Onodera, T. Koda, S. Sun, Angew. Chem. Int. Ed. **47**, 3588–3591 (2008)
14. S. Mostafa, F. Behafarid, J.R. Croy, L.K. Ono, L. Li, J.C. Yang, A.I. Frenkel, B.R. Cuenya, J. Am. Chem. Soc. **132**, 15714–15719 (2010)
15. R. Narayanan, M.A. El-Sayed, J. Am. Chem. Soc. **126**, 7194–7195 (2004)
16. Y. Liu, J. Chung, Y. Jang, S. Mao, B.M. Kim, Y. Wang, X. Guo, ACS Appl. Mater. Interfaces **6**, 1887–1892 (2014)
17. A. Balouch, A. Ali Umar, E.R. Mawarnis, S.K. Md Saad, M. Mat Salleh, M.Y. Abd Rahman, I.V. Kityk, M. Oyama, ACS Appl. Mater. Interfaces **7**, 7776–7785 (2015)
18. H. Ataee-Esfahani, Y. Nemoto, L. Wang, Y. Yamauchi, Chem. Commun. **47**, 3885–3887 (2011)
19. Y. Xia, Y. Xiong, B. Lim, S.E. Skrabalak, Angew. Chem. Int. Ed. **48**, 60–103 (2009)
20. B.C. Tappan, S.A. Steiner III, E.P. Luther, Angew. Chem. Int. Ed. **49**, 4544–4565 (2010)
21. R.M. Crooks, M. Zhao, L. Sun, V. Chechik, L.K. Yeung, Acc. Chem. Res. **34**, 181–190 (2001)
22. W. She, T. Qi, M. Cui, P. Yan, S.W. Ng, W. Li, G. Li, ACS Appl. Mater. Interfaces **10**, 14698–14707 (2018)
23. Y.-F. Jiang, C.-Z. Yuan, X. Xie, X. Zhou, N. Jiang, X. Wang, M. Imran, A.-W. Xu, ACS Appl. Mater. Interfaces **9**, 9756–9762 (2017)
24. M. Crespo-Quesada, A. Yarulin, M. Jin, Y. Xia, L. Kiwi-Minsker, J. Am. Chem. Soc. **133**, 12787–12794 (2011)
25. J. Xia, G. He, L. Zhang, X. Sun, X. Wang, Appl. Catal. B Environ. **180**, 408–415 (2016)
26. H.-Y. Hsueh, C.-T. Yao, R.-M. Ho, Chem. Soc. Rev. **44**, 1974–2018 (2015)
27. H.-F. Wang, L.-H. Yu, X.-B. Wang, R.-M. Ho, Macromolecules **47**, 7993–8001 (2014)
28. T.-C. Lin, K.-C. Yang, P. Georgopanos, A. Avgeropoulos, R.-M. Ho, Polymer **126**, 360–367 (2017)
29. H.-Y. Hsueh, Y.-C. Huang, R.-M. Ho, C.-H. Lai, T. Makida, H. Hasegawa, Adv. Mater. **23**, 3041–3046 (2011)
30. K.-C. Yang, C.-T. Yao, L.-Y. Huang, J.-C. Tsai, W.-S. Hung, H.-Y. Hsueh, R.-M. Ho, NPG Asia Materials **11**, 9 (2019)
31. S. Samitsu, R. Zhang, X. Peng, M.R. Krishnan, Y. Fujii, I. Ichinose, Nat. Commun. **4**, 2653 (2013)
32. X. He, W. Zhong, C.-T. Au, Y. Du, Nanoscale Res. Lett. **8**, 446 (2013)
33. J.C.V.D. Werff, C.G.D. Kruif, *J. Rheol.* **33**, 421–454 (1989)
34. K. Ito, H. Nakanishi, Y. Ujihira, J. Phys. Chem. B **103**, 4555–4558 (1999)
35. W.-S. Hung, Q.-F. An, C.-C. Hu, K.-R. Lee, Y.-C. Jean, J.-Y. Lai, RSC Adv. **6**, 85019–85025 (2016)
36. D. Shi, R. Wojcieszak, S. Paul, E. Marceau, Catalysts **9**, 451 (2019)
37. M. Matsuyama, K. Ashida, O. Takayasu, T. Takeuchi, J. Catal. **102**, 309–315 (1986)
38. P.S. Kumbhar, M.R. Kharkar, G.D. Yadav, R.A. Rajadhyaksha, J. Chem. Soc., Chem. Commun **7**, 584–586 (1992)
39. H. Littman, H. Bliss, Ind. Eng. Chem. **51**, 659–662 (1959)
40. Y. Wang, X. Cui, Y. Deng, F. Shi, RSC Adv. **4**, 2729–2732 (2014)